

Geophysical Research Letters®

RESEARCH LETTER

10.1029/2023GL102846

Key Points:

- Externally forced changes to wind-driven ocean circulation accelerate global warming by 17% in a coupled climate model
- The Antarctic Circumpolar Current and Pacific Ocean circulations are influenced by externally forced wind stress changes
- Externally forced changes to wind-driven ocean circulation amplify Southern Hemisphere warming

Supporting Information:

Supporting Information may be found in the online version of this article.

Correspondence to:

K. McMonigal,
ktmcmoni@ncsu.edu

Citation:

McMonigal, K., Larson, S., Hu, S., & Kramer, R. (2023). Historical changes in wind-driven ocean circulation can accelerate global warming. *Geophysical Research Letters*, 50, e2023GL102846. <https://doi.org/10.1029/2023GL102846>

Received 10 JAN 2023

Accepted 13 FEB 2023

Author Contributions:

Conceptualization: Sarah Larson
Funding acquisition: Sarah Larson
Investigation: Ryan Kramer
Methodology: Shineng Hu
Project Administration: Sarah Larson
Resources: Sarah Larson
Supervision: Sarah Larson
Validation: Ryan Kramer
Visualization: Shineng Hu
Writing – review & editing: Sarah Larson, Shineng Hu, Ryan Kramer

© 2023 The Authors.

This is an open access article under the terms of the Creative Commons Attribution-NonCommercial License, which permits use, distribution and reproduction in any medium, provided the original work is properly cited and is not used for commercial purposes.

Historical Changes in Wind-Driven Ocean Circulation Can Accelerate Global Warming

Kay McMonigal¹ , Sarah Larson¹ , Shineng Hu² , and Ryan Kramer^{3,4} 

¹Department of Marine, Earth, and Atmospheric Sciences, North Carolina State University, Raleigh, NC, USA, ²Division of Earth and Climate Sciences, Nicholas School of the Environment, Duke University, Durham, NC, USA, ³Climate and Radiation Laboratory, Earth Sciences Division, NASA Goddard Space Flight Center, Greenbelt, MD, USA, ⁴Goddard Earth Science Technology Research II, University of Maryland Baltimore County, Baltimore, MD, USA

Abstract Mitigation and adaptation strategies for climate change depend on accurate climate projections for the coming decades. While changes in radiative heat fluxes are known to contribute to surface warming, changes to ocean circulation can also impact the rate of surface warming. Previous studies suggest that projected changes to ocean circulation reduce the rate of global warming. However, these studies consider large greenhouse gas forcing scenarios, which induce a significant buoyancy-driven decline of the Atlantic Meridional Overturning Circulation. Here, we use a climate model to quantify the previously unknown impact of changes to wind-driven ocean circulation on global surface warming. Wind-driven ocean circulation changes amplify the externally forced warming rate by 17% from 1979 to 2014. Accurately simulating changes to the atmospheric circulation is key to improving near-term climate projections.

Plain Language Summary Global warming of surface air temperature is largely due to increases in greenhouse gases, which lead to increased radiative heat fluxes toward Earth's surface. However, the exact pattern and rate of global warming are also influenced by the uptake and redistribution of heat by the ocean, which can be altered by warming. Previous studies have quantified the role of the changing ocean circulation as a whole on the rate and pattern of global warming. However, the relative contribution of different ocean dynamical processes has not been explored yet. Ocean circulation can broadly be divided into components driven by wind and density differences. Here, we quantify the role of changes to the wind-driven ocean circulation onto global air temperature warming. We find that changes to the wind-driven ocean circulation amplify global warming by 17% from 1979 to 2014. Climate models need to adequately simulate changes to the winds, and the ocean's response to these wind changes, to accurately project climate change.

1. Introduction

Anthropogenic forcing is expected to alter the atmospheric circulation as a response to increased net absorbed radiative heat fluxes (Held & Soden, 2006; Lu et al., 2008; Vecchi & Soden, 2007). The adjustment of the atmospheric circulation to anthropogenic forcing can then impact the ocean circulation by altering winds or buoyancy fluxes, two major drivers of the large-scale ocean circulation. The large-scale ocean circulation plays a key role in setting the spatially varying pattern of sea surface temperature (SST) warming by redistributing the heat taken up by the ocean from increased downward heat flux (Banks & Gregory, 2006; Hu et al., 2020, 2022; Liu et al., 2018; Lyu et al., 2020). This pattern of SST warming can feed back onto the atmosphere through pattern-dependent radiative feedbacks, largely linked to cloud-SST feedbacks (termed “the pattern effect”; Armour, 2017; Armour et al., 2013; Dong et al., 2019, 2020; Rose et al., 2014; Stevens et al., 2016). Therefore, changes to the atmospheric circulation that drive a change in ocean circulation could alter the globally averaged rate of anthropogenic warming.

Externally forced changes to the atmospheric circulation, and the impacts of these changes onto the oceanic circulations, have already begun to occur over the historical record. The Southern Hemisphere midlatitude winds have increased over the past four decades (Thompson et al., 2011; Thompson & Solomon, 2002), altering the wind-driven circulation in the South Indian and South Pacific subtropical gyres (Beal & Eliot, 2016; Lee et al., 2015; McMonigal et al., 2018, 2022; Palmer et al., 2004; Roemmich et al., 2007, 2016). In the tropical Pacific, the trade winds have increased in strength (M. H. England et al., 2014; McGregor et al., 2012; Merrifield et al., 2012; Timmermann et al., 2010), leading to cooling in the equatorial Pacific (Seager et al., 2022).

Previous studies have quantified the role of the ocean circulation on the rate of anthropogenic warming under high emissions scenarios, such as a doubling or quadrupling of CO₂ (Garuba et al., 2018; Trossman et al., 2016; Winton et al., 2013). In these scenarios, the projected decline of the Atlantic Meridional Overturning Circulation (AMOC) dominates the oceanic response of the climate system, by cooling the high latitude North Atlantic and allowing for increased deep ocean heat uptake within the North Atlantic (Rugenstien et al., 2013). This leads to a decrease in the globally averaged surface warming; thus, the overall role of the ocean is to mediate the surface warming rate. Beyond the impacts from AMOC decline, whether externally forced changes in the wind-driven ocean circulation mediate or amplify the warming rate is relatively unexplored despite its potential influence on regional scales. Moreover, developing mitigation and adaptation strategies relies on accurate near-term (20–40 years) climate projections (Hewitt & Lowe, 2018; Nissan et al., 2019), a timescale over which large AMOC trends are not expected (Lobelle et al., 2020; Weijer et al., 2020).

In this study, we quantify the role of externally forced changes to the wind-driven ocean from 1979 to 2014 in the Community Earth System Model version 2 (CESM2). We isolate this effect by comparing two large ensembles within CESM2: one including the role of changes to the wind-driven ocean circulation, and the other excluding it. Crucially, the effect of changes in the wind-driven ocean circulation is opposite in sign to the role of ocean circulation on global warming under higher emission scenarios (Garuba et al., 2018; Trossman et al., 2016; Winton et al., 2013). This implies that the role of the changing ocean circulation on the globally averaged rate of surface warming depends on the ocean dynamics at play, with opposing roles of boundary-driven ocean circulation changes like AMOC, and wind-driven ocean circulation changes.

2. Methods

2.1. Experimental Design

We use two CESM2 ensembles forced by realistic, time-varying 1850–2014 external forcing, including greenhouse gasses, anthropogenic aerosol emissions, natural aerosols (e.g., volcanic), and solar irradiance. In the first ensemble, referred to as FCM for “Fully Coupled Model,” the ocean and atmosphere exchange time-varying buoyancy and wind stress (momentum) fluxes. In the second ensemble, referred to as MDM for “Mechanically Decoupled Model,” the ocean and atmosphere exchange time-varying buoyancy fluxes, but the ocean is forced by a fixed wind stress climatology, calculated from preindustrial conditions. The atmospheric winds in MDM vary in time; only the wind stress forcing onto the ocean is fixed to a climatology. Both models have similar preindustrial mean climates and ocean circulation (Figures S1–S3 in Supporting Information S1). Additionally, because the low frequency, interhemispheric component of AMOC is predominantly buoyancy forced (Biastoch et al., 2008; Medhaug et al., 2012; Polo et al., 2014; Yeager & Danabasoglu, 2014), FCM and MDM simulate similar AMOC mean states (Larson et al., 2020), similar externally forced declines in AMOC (Figure 1a), and similar externally forced trends in ocean meridional heat transport (Figure 1b).

To isolate the externally forced trends, we compute the ensemble mean linear trends in each simulation to remove the internal variability (Bengtsson & Hodges, 2019; Deser et al., 2012, 2020; Hawkins et al., 2016; Machete & Smith, 2016). The difference between the ensemble mean trends in the FCM and MDM isolates climate changes due to externally forced trends in the wind-driven ocean circulation. We refer to this component of the trends as due to the dynamic response of the ocean to changes in the “Winds,” as we expect the total forced trend to be a linear superposition of wind and buoyancy forced trends (Fyfe et al., 2007; Yeager & Danabasoglu, 2014). In this coupled model setup, ocean circulation trends can feedback onto the atmosphere, sea ice, and land.

2.2. Model Ensembles

Both FCM and MDM ensembles were run using the smoothed biomass-burning setup of the CESM2 (Danabasoglu et al., 2020; Fasullo et al., 2022; Rodgers et al., 2021). This model consists of the Community Atmosphere Model version 6, the Parallel Ocean Project version 2 (Smith et al., 2010), the Community Land Model version 5 (Lawrence et al., 2019), and the Los Alamos Community Ice Code version 5 (Hunke et al., 2017). The model components communicate through the Common Infrastructure for Modeling the Earth (CIME) coupler. The alteration of the wind stress forcing passed to the ocean in the MDM ensemble is done within CIME, by overwriting the time-varying wind stress forcing passed from the atmosphere to the ocean. Both models were forced by realistic 1850–2014 greenhouse gas emissions.

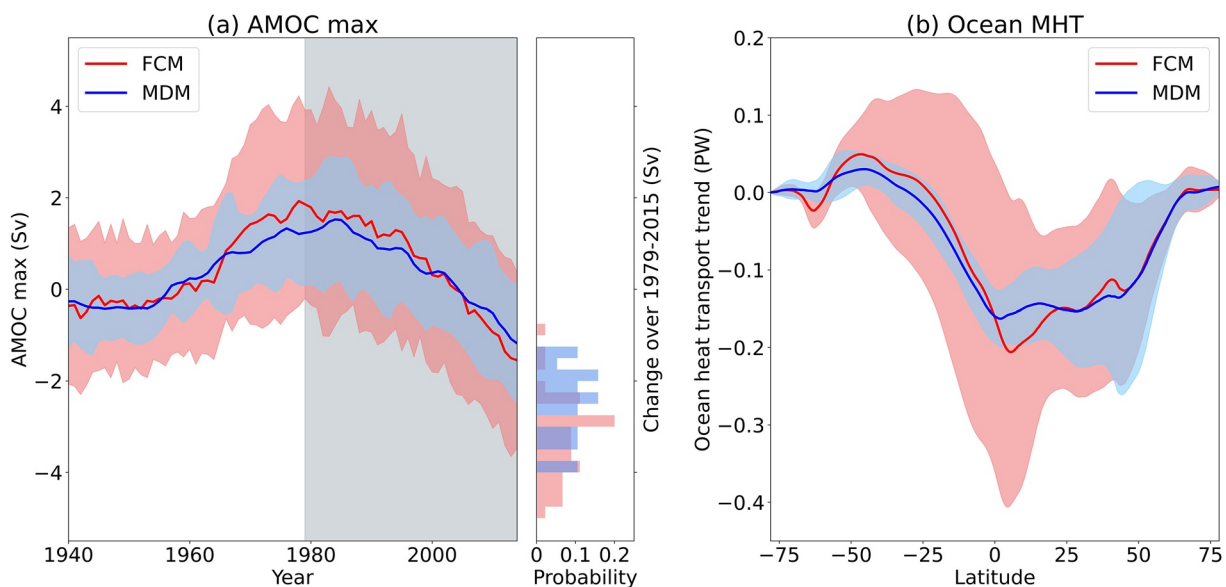


Figure 1. (a) Ensemble mean Atlantic Meridional Overturning Circulation (AMOC) intensity in each simulation (thick lines) with two standard deviation shading. Histogram shows trends from 1979 to 2014 in each ensemble member. (b) Ensemble mean trends in ocean meridional heat transport (MHT; thick lines) with two standard deviation shading.

CESM2 is a part of CMIP6. In CMIP6, stratospheric ozone trends are prescribed, but no tropospheric ozone trends are included (Liu et al., 2022). Anthropogenic aerosols are prescribed, and lead to an SST cooling that is similar in structure to the greenhouse gas-induced warming (Xie et al., 2013) but show distinct regional patterns in surface wind trends (Wang et al., 2016). CESM2 has a horizontal ocean resolution of approximately 1°.

The FCM ensemble was created by branching 50 ensemble members from a spun-up, preindustrial model run for more than 1,000 years. This includes 10 macro ensemble members, where each of the members is branched from a different preindustrial climate state, and four sets of 10 micro ensemble members, where each set of micro ensemble members is branched from a different preindustrial climate, and each ensemble member is created by adding a random, round off error level perturbation to the atmospheric potential temperature field.

The MDM ensemble was created by branching 20 ensemble members from a spun-up, preindustrial MDM model run. The wind stress climatology forcing in the MDM runs was calculated from 50 years of the FCM preindustrial run. Each ensemble member was branched from a different year of the preindustrial MDM run, making it a macro ensemble.

The FCM and MDM preindustrial runs have similar mean states. In the preindustrial run, SSTs are warmer and mixed layer depths are shallower in MDM (Figures S1 and S2 in Supporting Information S1). The ocean circulation mean state is similar in the two models, in all regions except the Southern Ocean (Figure S3 in Supporting Information S1). MDM has a stronger Antarctic Circumpolar Current, likely due to alterations of the isopycnals across the Southern Ocean.

2.3. Observational Data

For comparison to the modeled trends, observational trends were estimated by using GISS Surface Temperature Anomaly version 4 (GISTEMP) surface air temperature and ECMWF reanalysis version 5 (ERA5) wind stress.

2.4. Analyses

To analyze the globally averaged surface temperature response, we consider the ensemble mean reference height air temperature. AMOC max is calculated as the maximum AMOC stream function between 20° and 65°N, at each time step. All trends shown are linear trends calculated from annual mean anomalies from the climatology calculated over the 1941–1970 period, to remove any dependence on mean state differences. Trends are multiplied

by the length of the time period, to give units that match the variable of interest. Top-of-atmosphere (TOA) total radiation, longwave radiation, and shortwave radiation are defined as positive downward. For the radiative flux regressions shown in Figure S10 in Supporting Information S1, the earlier time period trends are calculated as the linear trends over 1966–1987, excluding 1975, 1982, and 1983. This is due to the large volcanic influence during the 3 excluded years. The later time period trends are calculated as the linear trends over 1996–2014, to avoid the large volcanic influence of Mt. Pinatubo in 1991.

2.5. Significance Testing

To determine the regions and time periods where trends are significantly different, we consider the spread of the ensemble members as a normal distribution. To test if the distributions are significantly different, we calculate the Z statistic and use 95% significance ($Z \geq 1.96$) as a threshold, where:

$$Z = \frac{X_{\text{FCM}} - X_{\text{MDM}}}{\sqrt{\sigma_{\text{FCM}}^2 - \sigma_{\text{MDM}}^2}}$$

X is the ensemble mean from each simulation. σ is the standard deviation of each ensemble member divided by the square root of the number of ensemble members.

The global mean temperature difference is also significant at the 95% level when considering temporal correlations of residuals of the difference of ensemble means, following (Santer et al., 2000).

3. Wind Stress and Wind-Driven Ocean Circulation Trends

Externally forced changes to the wind stress primarily manifest within the Southern Hemisphere westerlies and the Pacific trades and North Pacific westerlies (Figure 2a). The Southern Hemisphere westerlies strengthen and shift poleward beginning in 1970 (Figure S4 in Supporting Information S1) and broadly agree with reanalysis product wind stress trends in the region (Figure S5 in Supporting Information S1). The strengthening and shifting of the Southern Hemisphere westerlies have been linked to both stratospheric ozone and greenhouse gas forcing (Thompson et al., 2011; Thompson & Solomon, 2002). The Pacific trades and North Pacific westerlies weaken beginning in 1990 (Figure S4 in Supporting Information S1). The weakening of the Pacific trades is inconsistent with reanalysis products (M. H. England et al., 2014; McGregor et al., 2012; Merrifield et al., 2012; Timmermann et al., 2010), while the weakening of the North Pacific westerlies broadly matches the reanalysis product trend (Figure S5 in Supporting Information S1).

These wind stress trends lead to externally forced changes in the horizontal barotropic ocean circulation (BSF) over 1979–2014 (Figure 2c; mean barotropic stream function shown in Figure S6 in Supporting Information S1). The Antarctic Circumpolar Current accelerates due to wind stress trends, in agreement with the observed acceleration of Antarctic Circumpolar Current velocities (Shi et al., 2021). The tropical and North Pacific circulations weaken. Trends in the barotropic circulation are generally similar to trends in ocean currents averaged over the upper 150 m (Figure S7 in Supporting Information S1).

Comparing the role of buoyancy (illustrated by the MDM trend) and wind stress forcing (illustrated by the Winds trend) on externally forced changes in the BSF shows that buoyancy forcing dominates the changes in the Atlantic Ocean (Figures 2b and 2c). The buoyancy-forced weakening of the North Atlantic circulation is consistent with the simulated decline in the interhemispheric AMOC in the model (Figure 1a). Although the simulated AMOC decline is similar in both models, a significantly larger decline of 3.5 Sv is seen in FCM, while MDM simulates a decline of 2.6 Sv. This suggests that, although buoyancy forcing dominates the forced AMOC decline, the changes in surface wind stress act to enhance the AMOC decline by about 25%. Both buoyancy and wind stress changes contribute to a weakening of the South Indian Ocean subtropical gyre. This is the opposite sign of the observed strengthening of the Southern Hemisphere gyres (McMonigal et al., 2018; Palmer et al., 2004; Roemmich et al., 2007, 2016), suggesting that the model may be biased or low-frequency internal variability projects onto the observed trends. Both buoyancy and wind stress changes contribute to changes in the Antarctic Circumpolar Current strength, although with opposite signs. Wind stress changes accelerate the Antarctic Circumpolar Current, while buoyancy changes slightly weaken it. This is opposite to the role of buoyancy forcing found under stronger greenhouse gas forcing (Peng et al., 2022; Shi et al., 2020). This suggests that the response of the Southern Ocean to buoyancy forcing may depend on the timescale or magnitude of forcing.

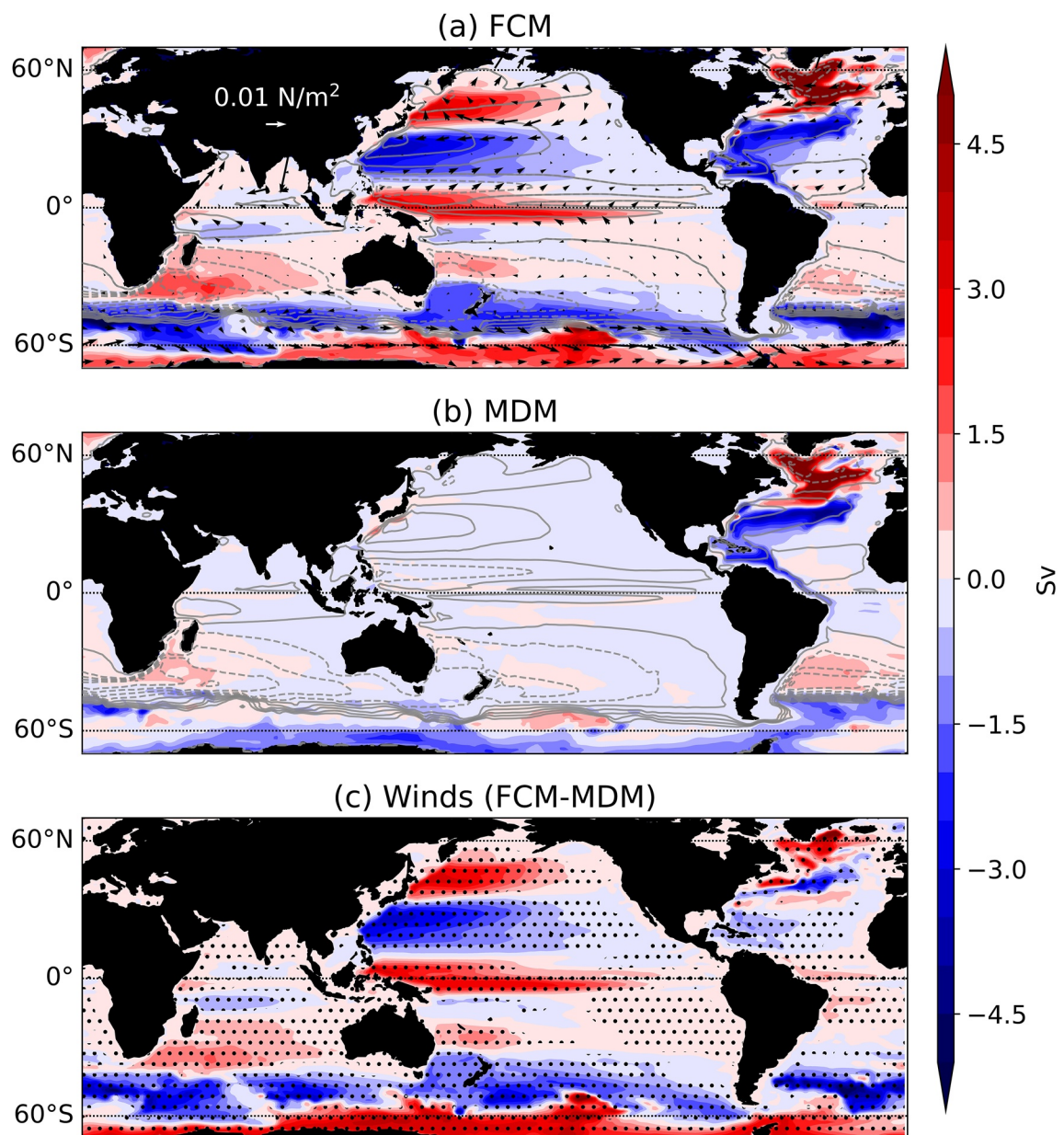


Figure 2. (a) Trend in FCM ensemble mean barotropic stream function (BSF) over 1979–2014 (colored contours) and wind stress (arrows). Gray contours show the 1941–1970 mean BSF, with contour values every 15 Sv from -75 to 60 Sv. (b) Trend in MDM ensemble mean barotropic stream function over 1979–2014 (colored contours) and wind stress (arrows). Gray contours show the 1941–1970 mean BSF, with contour values every 15 Sv from -75 to 60 Sv. (c) Winds ensemble mean trends. Stippling shows where FCM and MDM ensemble mean trends are significantly different. For all panels, negative values indicating counterclockwise circulation are dashed and positive values indicating clockwise circulation are solid.

Overall, the modeled externally forced acceleration of the Antarctic Circumpolar Current due to changes in the overlying westerlies is in agreement with atmospheric and oceanic observations. The weakening of the Pacific circulations due to weakening of the overlying winds is not corroborated by atmospheric reanalysis products.

4. Wind-Driven Ocean Circulation Trend Feedbacks

Global mean surface temperature anomalies are very similar with and without wind-driven ocean circulation changes, until the 1970s (Figure 3a). Trends in the wind stress forcing on the ocean lead to statistically significant global mean surface warming differences in the early 1990s (Figure 3b). This is several decades after

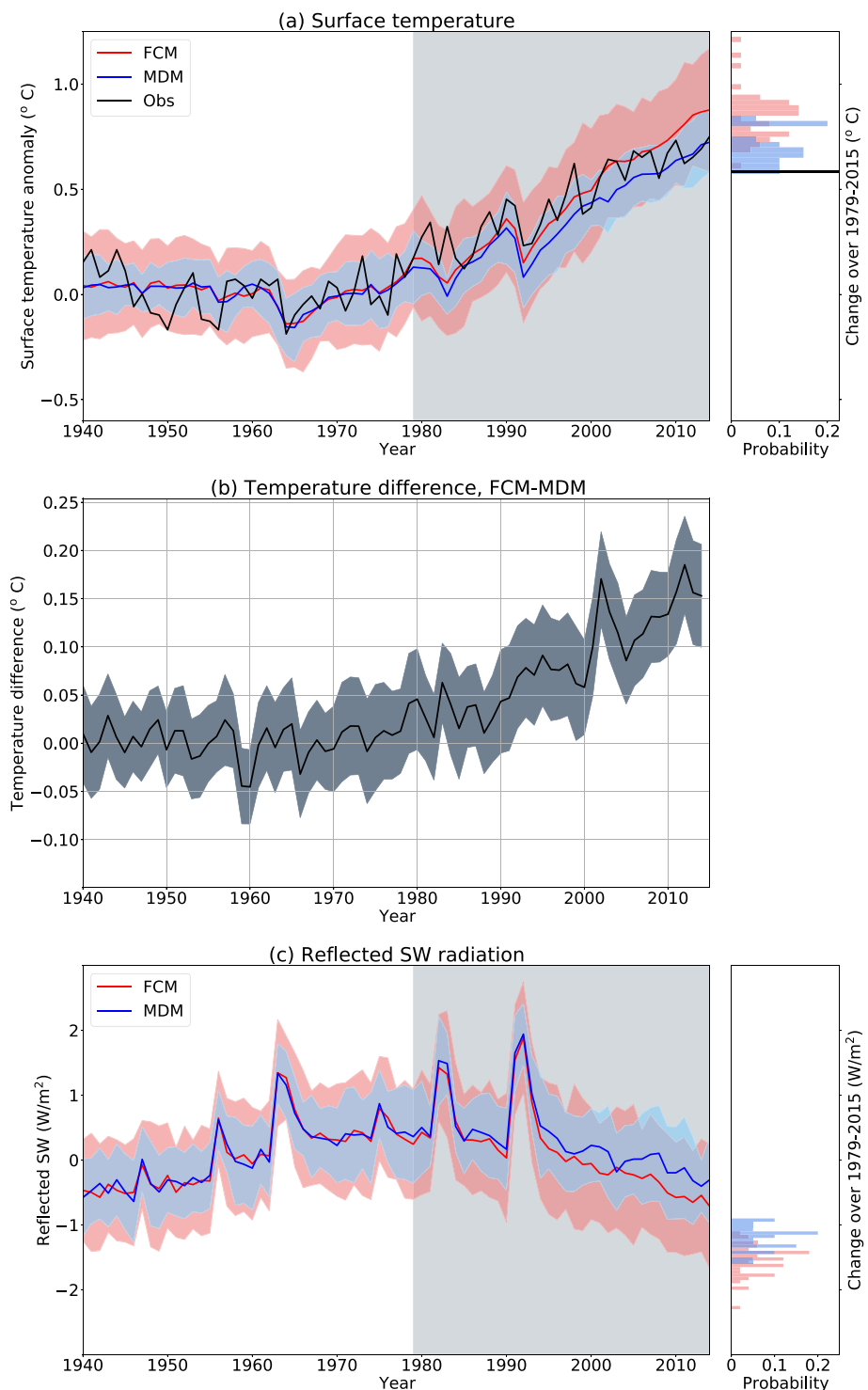


Figure 3. (a) Surface air temperature anomalies, with red showing FCM and blue showing MDM. Thick lines are ensemble means. Shading shows 2 standard deviations across ensemble members. Thick black line shows the GISTEMP observational product. Right-hand side histograms show the trend over 1979–2015 multiplied by the time period, to yield the change of each field. (b) The FCM-MDM temperature difference, with shading showing the 95% confidence interval. (c) Same as (a) but for global mean all sky top-of-atmosphere upward shortwave radiation anomalies.

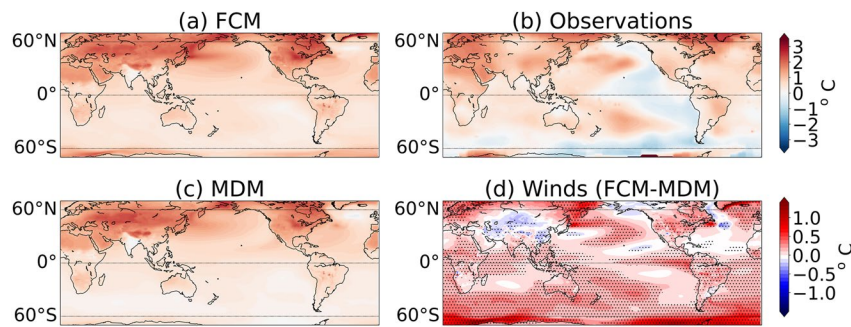


Figure 4. (a) Ensemble mean trend in surface air temperature over 1979–2014 in FCM. (b) Same but for GISTEMP observational product (c) Same but for MDM. (d) Same but for Winds. Stippling in bottom right is where FCM and MDM ensemble means are statistically different.

changes in the Southern Ocean winds, and temporally aligned with changes to the Pacific trade winds (Figure S4 in Supporting Information S1). Changes to the wind stress-driven ocean circulation lead to increased global warming of 0.15°C , or 17% of the trend in FCM (Table S1 in Supporting Information S1). The observed rate of global surface temperature change (0.59°C) is within the range of the MDM ensemble and is slightly colder than the range of possibilities simulated by the FCM ensemble. To understand the cause of the amplified warming in FCM compared to MDM, we first focus on the differences in the warming patterns between the two simulations.

Changes in the wind-driven ocean circulation lead to more warming over the Southern Hemisphere and the eastern tropical Pacific (Figure 4d). In both regions, models commonly show too much warming as compared to observations (Fan et al., 2014; Seager et al., 2022; Turner et al., 2013). In these regions, the MDM simulation shows better agreement with observations as compared to the more realistic FCM simulation, suggesting that a component of the model biases could be due to incorrect wind stress trends or incorrect ocean response to wind stress trends. In the Northern Hemisphere, trends in wind stress forcing shift warming patterns, including a zonal shift of the North Atlantic warming hole and a meridional shift of the simulated location of maximum warming in the North Pacific. Trends in wind stress forcing also significantly alter surface temperature trends over land, leading to a faster warming rate over much of the Americas, Europe, Africa, and Australia and slower warming over parts of Asia.

As an initial assessment of the dynamics leading to the warming pattern in Winds, we compare the surface air temperature trend (Figure 4d) to the upper 2,000 m ocean heat content (OHC) trend (Figure S8c in Supporting Information S1) and the mixed layer depth trend (Figure S9c in Supporting Information S1). Changes to the wind-driven ocean circulation lead to more OHC warming (greater surface heat fluxes into the ocean) in the Southern Hemisphere, North Atlantic, and high latitude North Pacific, and less OHC warming (surface heat fluxes out of the ocean) in the tropical Pacific. In the zonal mean, heat flux into the ocean is larger in FCM than MDM in the subtropics, while near the equator, FCM has surface heat fluxes out of the ocean while MDM has surface heat fluxes into the ocean (Figure S10a in Supporting Information S1). Changes to the wind-driven ocean circulation lead to a deeper mixed layer depths in the Southern Ocean and high latitude North Atlantic. Therefore, in the Southern Ocean, warmer surface temperatures in Winds are collocated with regions of larger OHC warming (Figure S8 in Supporting Information S1) and deeper mixed layers (Figure S9 in Supporting Information S1), suggesting that atmospheric processes may dominate. In contrast, in the tropical Pacific, Winds show amplified air temperature warming, reduced OHC warming, surface heat fluxes out of the ocean, and an altered mixed layer depth gradient across the basin (Figures S8 and S9 in Supporting Information S1). This suggests that dynamic oceanic processes dominate the wind-driven warming seen in the Pacific. Further study using regional heat budgets will elucidate specific dynamics at play.

The different warming patterns in each simulation could drive the different globally averaged warming rates through ocean heat uptake differences, or through differences in radiative feedbacks which alter the TOA radiation balance. Specifically, when comparing two simulations with the same external forcing, the simulation with a faster global warming rate must either have smaller ocean heat uptake or larger net radiative energy absorption by the planet (i.e., a larger TOA radiation imbalance) than the simulation with a slower global warming rate. The zonally averaged ocean heat uptake patterns in FCM and MDM are different, especially in the tropics where

FCM takes up less heat than MDM (Figure S10a in Supporting Information S1), which likely plays a role in the different zonal mean rates of surface warming (Figure S10b in Supporting Information S1) and differing values of ocean heat uptake efficiency (Table S1 in Supporting Information S1). Globally averaged, however, FCM warms more than MDM while also taking up more heat into the ocean (Table S1 in Supporting Information S1). Therefore, ocean heat uptake cannot explain the amplified warming in FCM. Instead, radiative fluxes, which are known to be dependent on the pattern of surface warming, lead to the amplification of the globally averaged warming rate in FCM. FCM begins to warm faster than MDM in about 1990 (Figure 3c), and so we focus the next analyses on the period 1995–2014.

Over 1995–2014, the all-sky, TOA radiation imbalance in FCM increases at a faster rate than in MDM (Figure S10c in Supporting Information S1), signifying the planet is gaining radiative energy at a faster rate in FCM than in MDM. This increase in radiative energy occurs in shortwave radiation under all-sky conditions but not in clear-sky conditions (Figure S10f in Supporting Information S1) nor in longwave radiation under all-sky conditions (Figure S10e in Supporting Information S1), suggesting shortwave cloud radiative effects explain the difference in the overall net radiative trends between FCM and MDM. In context of the different SST warming patterns between the simulations, we expect to see different net radiative trends. The amplified warming beginning in 1995 is consistent with when the Pacific trades weaken in FCM, leading to increased warming in the eastern equatorial Pacific (Figure 4d) through ocean dynamical processes. Anomalous SST warming in the eastern tropical Pacific is known to decrease the lower tropospheric stability and reduce low clouds locally (Andrews et al., 2015; Andrews & Webb, 2018; Cepi & Gregory, 2017; Zhou et al., 2017), thereby reducing the global reflected shortwave radiation (Figure 3c) and resulting in an increased downward TOA radiation imbalance (Figure S10c in Supporting Information S1). These results suggest that the weakening of the Pacific trades may play a larger role than the poleward intensified Southern Hemisphere westerlies in the amplification of global surface warming in FCM. However, it is possible that regional warming differences in the Southern Hemisphere are more impacted by the Southern Hemisphere westerly changes than the Pacific trade changes. Additionally, the Southern Hemisphere westerly wind shift and the weakened Pacific trades could be indirectly linked through an extratropical to tropical teleconnection (Dong et al., 2022; M. R. England et al., 2020).

5. Conclusions

Our study demonstrates that the wind-driven ocean circulation plays a critical role in pacing the global warming rate over 1979–2014 in a CMIP6 model, under realistic greenhouse gas and aerosol forcing. Externally forced changes to the wind-driven ocean circulation lead to increased surface warming of 0.15°C (17%). This increased warming is distributed as amplified warming over most of the Southern Hemisphere and a shifting of warming patterns in the Northern Hemisphere. The increased rate of warming caused by trends in wind-driven ocean is opposite in sign to the decreased rate of global warming due to ocean circulation changes found in previous studies (Garuba et al., 2018; Trossman et al., 2016; Winton et al., 2013). We hypothesize that this discrepancy is due to the different role of the AMOC decline, which dominates in studies that use large greenhouse gas forcings, and wind-driven ocean circulation changes which are isolated in our experimental setup. This suggests that the role of ocean circulation changes on global surface warming is dependent on dynamics and that at any point in time, the competing effects of an AMOC decline-driven cooling and a wind-driven ocean circulation warming dictate the total role of ocean circulation changes on surface warming. If this hypothesis is correct, ocean circulation changes could be contributing to time variability in the climate feedback parameter (Andrews et al., 2015). Over long time periods, AMOC decline likely dominates the oceanic warming feedback, and reduces global surface warming, whereas over shorter time scales (like those investigated here), wind-driven ocean circulation changes can amplify surface warming.

Wind-driven ocean circulation changes amplify SST warming in the eastern tropical Pacific, which feeds back onto the TOA radiation imbalance and leads to amplified global surface warming. What this means for the climate system depends on whether the wind stress trends in coupled models are systematically biased. Coupled climate models commonly simulate inaccurate SST trends in the eastern tropical Pacific (Seager et al., 2019, 2022), which can lead to global biases through cloud-SST feedback (Dong et al., 2021). Under this interpretation, biased wind stress trends or an incorrectly simulated oceanic response to the wind stress trends may be driving an overestimate of the rate of global surface warming. On the other hand, it is possible that the model-bias mismatch in the eastern tropical Pacific is due to natural variability, which offsets the forced trend isolated by model ensembles

(Bordbar et al., 2017; Olonscheck et al., 2020; Watanabe et al., 2021). This interpretation would imply that the role of wind-driven ocean circulation changes could amplify the surface warming rate, once the eastern tropical Pacific internal variability changes phases. In either case, it is crucial to understand climate model behavior to ensure future climate model projections are accurate.

Data Availability Statement

CESM2 FCM output is available from the Earth System Grid Federation (ESGF; at <https://esgf-node.llnl.gov/search/cmip6/>) as part of the CESM2 Large Ensemble (LENS2; <https://www.cesm.ucar.edu/projects/community-projects/LENS2/>). GISTEMP output was obtained freely from the National Aeronautics and Space Administration (NASA) Goddard Institute for Space Studies (<https://data.giss.nasa.gov/gistemp/>). ERA5 output was obtained freely from the European Centre for Medium-Range Weather Forecasts (ECMWF; <https://www.ecmwf.int/en/forecasts/dataset/ecmwf-reanalysis-v5>). Data analyzed from the CESM2 MDM are available in the Zenodo data repository at <https://doi.org/10.5281/zenodo.7154374>. CESM2 MDM model source code changes and wind stress climatology forcing data sets are available in the Zenodo data repository at <https://doi.org/10.5281/zenodo.6678286>. Code to make the figures is available in the Zenodo data repository at <https://doi.org/10.5281/zenodo.7158684>.

Acknowledgments

The authors thank Nan Rosenbloom for assistance running the MDM ensemble, and Clara Deser and the organizers of CLIVAR pattern effect meeting for productive scientific discussions. This work is supported by NSF Grant AGS-1951713 (KM and SML) and NASA Grant 80NSSC22K1025 (SH). RK was supported by NOAA Award NA18OAR4310269 and NASA Grant 80NSSC21K1968. The authors also acknowledge the high-performance computing support from Cheyenne provided by NCAR's Computing and Information Services Lab, sponsored by NSF.

References

Andrews, T., Gregory, J. M., & Webb, M. J. (2015). The dependence of radiative forcing and feedback on evolving patterns of surface temperature change in climate models. *Journal of Climate*, 28(4), 1630–1648. <https://doi.org/10.1175/JCLI-D-14-00545.1>

Andrews, T., & Webb, M. J. (2018). The dependence of global cloud and lapse rate feedbacks on the spatial structure of tropical Pacific warming. *Journal of Climate*, 31(2), 641–654. <https://doi.org/10.1175/JCLI-D-17-0087.1>

Armour, K. C. (2017). Energy budget constraints on climate sensitivity in light of inconstant climate feedbacks. *Nature Climate Change*, 7(5), 331–335. <https://doi.org/10.1038/nclimate3278>

Armour, K. C., Bitz, C. M., & Roe, G. H. (2013). Time-varying climate sensitivity from regional feedbacks. *Journal of Climate*, 26(13), 4518–4534. <https://doi.org/10.1175/JCLI-D-12-00544.1>

Banks, H. T., & Gregory, J. M. (2006). Mechanisms of ocean heat uptake in a coupled climate model and the implications for tracer based predictions of ocean heat uptake. *Geophysical Research Letters*, 33(7), L07608. <https://doi.org/10.1029/2005GL025352>

Beal, L. M., & Eliot, S. (2016). Broadening not strengthening of the Agulhas Current since the early 1990s. *Nature*, 540(7634), 570–573. <https://doi.org/10.1038/nature19853>

Bengtsson, L., & Hodges, K. I. (2019). Can an ensemble climate simulation be used to separate climate change signals from internal unforced variability? *Climate Dynamics*, 52(5), 3553–3573. <https://doi.org/10.1007/s00382-018-4343-8>

Biastoch, A., Böning, C. W., Getzlaff, J., Molines, J.-M., & Madec, G. (2008). Causes of interannual–decadal variability in the meridional overturning circulation of the midlatitude North Atlantic ocean. *Journal of Climate*, 21(24), 6599–6615. <https://doi.org/10.1175/2008JCLI2404.1>

Bordbar, M. H., Martin, T., Latif, M., & Park, W. (2017). Role of internal variability in recent decadal to multidecadal tropical Pacific climate changes. *Geophysical Research Letters*, 44(9), 4246–4255. <https://doi.org/10.1002/2016GL072355>

Ceppi, P., & Gregory, J. M. (2017). Relationship of tropospheric stability to climate sensitivity and Earth's observed radiation budget. *Proceedings of the National Academy of Sciences of the United States of America*, 114(50), 13126–13131. <https://doi.org/10.1073/pnas.1714308114>

Danabasoglu, G., Lamarque, J. F., Bacmeister, J., Bailey, D. A., DuVivier, A. K., Edwards, J., et al. (2020). The Community Earth System Model Version 2 (CESM2). *Journal of Advances in Modeling Earth Systems*, 12(2), 1–35. <https://doi.org/10.1029/2019MS001916>

Deser, C., Lehner, F., Rodgers, K. B., Ault, T., Delworth, T. L., DiNezio, P. N., et al. (2020). Insights from Earth system model initial-condition large ensembles and future prospects. *Nature Climate Change*, 10(4), 277–286. <https://doi.org/10.1038/s41558-020-0731-2>

Deser, C., Phillips, A., Bourdette, V., & Teng, H. (2012). Uncertainty in climate change projections: The role of internal variability. *Climate Dynamics*, 38(3–4), 527–546. <https://doi.org/10.1007/s00382-010-0977-x>

Dong, Y., Armour, K. C., Battisti, D. S., & Blanchard-Wrigglesworth, E. (2022). Two-way teleconnections between the Southern Ocean and the tropical Pacific via a dynamic feedback. *Journal of Climate*, 35(19), 1–37. <https://doi.org/10.1175/JCLI-D-22-0080.1>

Dong, Y., Armour, K. C., Proistosescu, C., Andrews, T., Battisti, D. S., Forster, P. M., et al. (2021). Biased estimates of equilibrium climate sensitivity and transient climate response derived from historical CMIP6 simulations. *Geophysical Research Letters*, 48(24), e2021GL095778. <https://doi.org/10.1029/2021GL095778>

Dong, Y., Armour, K. C., Zelinka, M. D., Proistosescu, C., Battisti, D. S., Zhou, C., & Andrews, T. (2020). Intermodel spread in the pattern effect and its contribution to climate sensitivity in CMIP5 and CMIP6 models. *Journal of Climate*, 33(18), 7755–7775. <https://journals.ametsoc.org/view/journals/clim/33/18/jcliD191011.xml>

Dong, Y., Proistosescu, C., Armour, K. C., & Battisti, D. S. (2019). Attributing historical and future evolution of radiative feedbacks to regional warming patterns using a Green's function approach: The preeminence of the Western Pacific. *Journal of Climate*, 32(17), 5471–5491. <https://doi.org/10.1175/JCLI-D-18-0843.1>

England, M. H., McGregor, S., Spence, P., Meehl, G. A., Timmermann, A., Cai, W., et al. (2014). Recent intensification of wind-driven circulation in the Pacific and the ongoing warming hiatus. *Nature Climate Change*, 4(3), 222–227. <https://doi.org/10.1038/nclimate2106>

England, M. R., Polvani, L. M., Sun, L., & Deser, C. (2020). Tropical climate responses to projected Arctic and Antarctic sea-ice loss. *Nature Geoscience*, 13(4), 275–281. <https://doi.org/10.1038/s41561-020-0546-9>

Fan, T., Deser, C., & Schneider, D. P. (2014). Recent Antarctic sea ice trends in the context of Southern Ocean surface climate variations since 1950. *Geophysical Research Letters*, 41(7), 2419–2426. <https://doi.org/10.1002/2014GL059239>

Fasullo, J. T., Lamarque, J.-F., Hannay, C., Rosenbloom, N., Tilmes, S., DeRepentigny, P., et al. (2022). Spurious late historical-era warming in CESM2 driven by prescribed biomass burning emissions. *Geophysical Research Letters*, 49(2), e2021GL097420. <https://doi.org/10.1029/2021GL097420>

Fyfe, J. C., Saenko, O. A., Zickfeld, K., Eby, M., & Weaver, A. J. (2007). The role of poleward-intensifying winds on Southern Ocean warming. *Journal of Climate*, 20(21), 5391–5400. <https://doi.org/10.1175/2007JCLI1764.1>

Garuba, O. A., Lu, J., Liu, F., & Singh, H. A. (2018). The active role of the ocean in the temporal evolution of climate sensitivity. *Geophysical Research Letters*, 45(1), 306–315. <https://doi.org/10.1002/2017GL075633>

Hawkins, E., Smith, R. S., Gregory, J. M., & Stainforth, D. A. (2016). Irreducible uncertainty in near-term climate projections. *Climate Dynamics*, 46(11), 3871–3819. <https://doi.org/10.1007/s00382-015-2806-8>

Held, I. M., & Soden, B. J. (2006). Robust responses of the hydrological cycle to global warming. *Journal of Climate*, 19(21), 5686–5699. <https://doi.org/10.1175/JCLI3990.1>

Hewitt, C. D., & Lowe, J. A. (2018). Toward a European climate prediction system. *Bulletin of the American Meteorological Society*, 99(10), 1997–2001. <https://doi.org/10.1175/BAMS-D-18-0022.1>

Hunke, E., Lipscomb, W., Jones, P., Turner, A., Jeffery, N., & Elliott, S. (2017). *CICE, The Los Alamos Sea Ice Model (CICE; 005315WKSTN00)*. Los Alamos National Lab. (LANL). Retrieved from <https://www.osti.gov/biblio/1364126>

Hu, S., Xie, S. P., & Kang, S. M. (2022). Global warming pattern formation: The role of ocean heat uptake. *Journal of Climate*, 35(6), 1885–1899. <https://doi.org/10.1175/JCLI-D-21-0317.1>

Hu, S., Xie, S. P., & Liu, W. (2020). Global pattern formation of net ocean surface heat flux response to greenhouse warming. *Journal of Climate*, 33(17), 7503–7522. <https://doi.org/10.1175/JCLI-D-19-0642.1>

Larson, S. M., Buckley, M. W., & Clement, A. C. (2020). Extracting the buoyancy-driven Atlantic Meridional Overturning Circulation. *Journal of Climate*, 33(11), 4697–4714. <https://doi.org/10.1175/JCLI-D-19-0590.1>

Lawrence, D. M., Fisher, R. A., Koven, C. D., Oleson, K. W., Swenson, S. C., Bonan, G., et al. (2019). The Community Land Model Version 5: Description of new features, benchmarking, and impact of forcing uncertainty. *Journal of Advances in Modeling Earth Systems*, 11(12), 4245–4287. <https://doi.org/10.1029/2018MS001583>

Lee, S.-K., Park, W., Baringer, M. O., Gordon, A. L., Huber, B., & Liu, Y. (2015). Pacific origin of the abrupt increase in Indian Ocean heat content during the warming hiatus. *Nature Geoscience*, 8(6), 445–449. <https://doi.org/10.1038/ngeo2438>

Liu, W., Hegglin, M. I., Checa-Garcia, R., Li, S., Gillett, N. P., Lyu, K., et al. (2022). Stratospheric ozone depletion and tropospheric ozone increases drive Southern Ocean interior warming. *Nature Climate Change*, 12(4), 365–372. <https://doi.org/10.1038/s41558-022-01320-w>

Liu, W., Lu, J., Xie, S.-P., & Fedorov, A. (2018). Southern Ocean heat uptake, redistribution and storage in a warming climate: The role of meridional overturning circulation. *Journal of Climate*, 31(12), 4727–4743. <https://doi.org/10.1175/JCLI-D-17-0761.1>

Lobelle, D., Beaupied, C., Livina, V., Séville, F., & Frajka-Williams, E. (2020). Detectability of an AMOC decline in current and projected climate changes. *Geophysical Research Letters*, 47(20), e2020GL089974. <https://doi.org/10.1029/2020GL089974>

Lu, J., Chen, G., & Frierson, D. M. W. (2008). Response of the zonal mean atmospheric circulation to El Niño versus global warming. *Journal of Climate*, 21(22), 5835–5851. <https://doi.org/10.1175/2008JCLI2200.1>

Lyu, K., Zhang, X., Church, J. A., & Wu, Q. (2020). Processes responsible for the southern hemisphere ocean heat uptake and redistribution under anthropogenic warming. *Journal of Climate*, 33(9), 3787–3807. <https://doi.org/10.1175/JCLI-D-19-0478.1>

Machete, R. L., & Smith, L. A. (2016). Demonstrating the value of larger ensembles in forecasting physical systems. *Tellus A: Dynamic Meteorology and Oceanography*, 68(1), 28393. <https://doi.org/10.3402/tellusa.v68.28393>

McGregor, S., Gupta, A. S., & England, M. H. (2012). Constraining wind stress products with sea surface height observations and implications for Pacific Ocean sea level trend attribution. *Journal of Climate*, 25(23), 8164–9176. <https://doi.org/10.1175/JCLI-D-12-00105.1>

McMonigal, K., Beal, L. M., & Willis, J. K. (2018). The seasonal cycle of the South Indian Ocean subtropical gyre circulation as revealed by Argo and satellite data. *Geophysical Research Letters*, 45(17), 9034–9041. <https://doi.org/10.1029/2018GL078420>

McMonigal, K., Gunn, K. L., Beal, L. M., Eliot, S., & Willis, J. K. (2022). Reduction in meridional heat export contributes to recent Indian Ocean warming. *Journal of Physical Oceanography*, 52(3), 329–345. <https://doi.org/10.1175/JPO-D-21-0085.1>

Medhaug, I., Langehaug, H. R., Eldevik, T., Furevik, T., & Bentzen, M. (2012). Mechanisms for decadal scale variability in a simulated Atlantic Meridional Overturning Circulation. *Climate Dynamics*, 39(1), 77–93. <https://doi.org/10.1007/s00382-011-1124-z>

Merrifield, M. A., Thompson, P. R., & Lander, M. (2012). Multidecadal sea level anomalies and trends in the western tropical Pacific. *Geophysical Research Letters*, 39(13), L13602. <https://doi.org/10.1029/2012GL052032>

Nissan, H., Goddard, L., de Perez, E. C., Furlow, J., Baethgen, W., Thomson, M. C., & Mason, S. J. (2019). On the use and misuse of climate change projections in international development. *WIREs Climate Change*, 10(3), e579. <https://doi.org/10.1002/wcc.579>

Olonscheck, D., Rugenstein, M., & Marotzke, J. (2020). Broad consistency between observed and simulated trends in sea surface temperature patterns. *Geophysical Research Letters*, 47(10), e2019GL086773. <https://doi.org/10.1029/2019GL086773>

Palmer, M. D., Bryden, H. L., Hirschi, J., & Marotzke, J. (2004). Observed changes in the South Indian Ocean gyre circulation, 1987–2002. *Geophysical Research Letters*, 31(15), 2–5. <https://doi.org/10.1029/2004GL020506>

Peng, Q., Xie, S.-P., Wang, D., Huang, R. X., Chen, G., Shu, Y., et al. (2022). Surface warming-induced global acceleration of upper ocean currents. *Science Advances*, 8(16), eabj8394. <https://doi.org/10.1126/sciadv.abj8394>

Polo, I., Robson, J., Sutton, R., & Balmaseda, M. A. (2014). The importance of wind and buoyancy forcing for the boundary density variations and the geostrophic component of the AMOC at 26°N. *Journal of Physical Oceanography*, 44(9), 2387–2408. <https://doi.org/10.1175/JPO-D-13-0264.1>

Rodgers, K. B., Lee, S.-S., Rosenbloom, N., Timmermann, A., Danabasoglu, G., Deser, C., et al. (2021). Ubiquity of human-induced changes in climate variability. *Earth System Dynamics*, 12(4), 1393–1411. <https://doi.org/10.5194/esd-12-1393-2021>

Roemmich, D., Gilson, J., Davis, R., Sutton, P., Wijffels, S., & Riser, S. (2007). Decadal spinup of the South Pacific subtropical gyre. *Journal of Physical Oceanography*, 37(2), 162–173. <https://doi.org/10.1175/JPO3004.1>

Roemmich, D., Gilson, J., Sutton, P., & Zilberman, N. (2016). Multidecadal change of the South Pacific gyre circulation. *Journal of Physical Oceanography*, 46(6), 1871–1883. <https://doi.org/10.1175/JPO-D-15-0237.1>

Rose, B. E. J., Armour, K. C., Battisti, D. S., Feldl, N., & Koll, D. D. B. (2014). The dependence of transient climate sensitivity and radiative feedbacks on the spatial pattern of ocean heat uptake. *Geophysical Research Letters*, 41(3), 1071–1078. <https://doi.org/10.1002/2013GL058955>

Rugenstein, M. A. A., Winton, M., Stouffer, R. J., Griffies, S. M., & Hallberg, R. (2013). Northern high-latitude heat budget decomposition and transient warming. *Journal of Climate*, 26(2), 609–621. <https://doi.org/10.1175/JCLI-D-11-00695.1>

Santer, B. D., Wigley, T. M. L., Boyle, J. S., Gaffen, D. J., Hnilo, J. J., Nychka, D., et al. (2000). Statistical significance of trends and trend differences in layer-average atmospheric temperature time series. *Journal of Geophysical Research: Atmospheres*, 105(D6), 7337–7356. <https://doi.org/10.1029/1999JD901105>

Seager, R., Cane, M., Henderson, N., Lee, D.-E., Abernathay, R., & Zhang, H. (2019). Strengthening tropical Pacific zonal sea surface temperature gradient consistent with rising greenhouse gases. *Nature Climate Change*, 9(7), 517–522. <https://doi.org/10.1038/s41558-019-0505-x>

Seager, R., Henderson, N. L., & Cane, M. A. (2022). Persistent discrepancies between observed and modeled trends in the tropical Pacific Ocean. *Journal of Climate*, 35(14), 4571–4584. <https://doi.org/10.7916/6wd4-f378>

Shi, J. R., Talley, L. D., Xie, S. P., Liu, W., & Gille, S. T. (2020). Effects of buoyancy and wind forcing on Southern Ocean climate change. *Journal of Climate*, 33(23), 10003–10020. <https://doi.org/10.1175/JCLI-D-19-0877.1>

Shi, J. R., Talley, L. D., Xie, S. P., Peng, Q., & Liu, W. (2021). Ocean warming and accelerating Southern Ocean zonal flow. *Nature Climate Change*, 11(12), 1090–1097. <https://doi.org/10.1038/s41558-021-01212-5>

Smith, R., Jones, P., Briegleb, B., Bryan, F., Danabasoglu, G., Dennis, J., et al. (2010). The Parallel Ocean Program (POP) reference manual.

Stevens, B., Sherwood, S. C., Bony, S., & Webb, M. J. (2016). Prospects for narrowing bounds on Earth's equilibrium climate sensitivity. *Earth's Future*, 4(11), 512–522. <https://doi.org/10.1002/2016EF000376>

Thompson, D. W. J., & Solomon, S. (2002). Interpretation of recent Southern Hemisphere climate change. *Science*, 296(5569), 895–899. <https://doi.org/10.1126/science.1069270>

Thompson, D. W. J., Solomon, S., Kushner, P. J., England, M. H., Grise, K. M., & Karoly, D. J. (2011). Signatures of the Antarctic ozone hole in Southern Hemisphere surface climate change. *Nature Geoscience*, 4(11), 741–749. <https://doi.org/10.1038/ngeo1296>

Timmermann, A., McGregor, S., & Jin, F. F. (2010). Wind effects on past and future regional sea level trends in the southern Indo-Pacific. *Journal of Climate*, 23(16), 4429–4437. <https://doi.org/10.1175/2010JCLI3519.1>

Trossman, D. S., Palter, J. B., Merlis, T. M., Huang, Y., & Xia, Y. (2016). Large-scale ocean circulation–cloud interactions reduce the pace of transient climate change. *Geophysical Research Letters*, 43(8), 3935–3943. <https://doi.org/10.1002/2016GL067931>

Turner, J., Bracegirdle, T. J., Phillips, T., Marshall, G. J., & Hosking, J. S. (2013). An initial assessment of Antarctic Sea ice extent in the CMIP5 models. *Journal of Climate*, 26(5), 1473–1484. <https://doi.org/10.1175/JCLI-D-12-00068.1>

Vecchi, G. A., & Soden, B. J. (2007). Global warming and the weakening of the tropical circulation. *Journal of Climate*, 20(17), 4316–4340. <https://doi.org/10.1175/JCLI4258.1>

Wang, H., Xie, S.-P., & Liu, Q. (2016). Comparison of climate response to anthropogenic aerosol versus greenhouse gas forcing: Distinct patterns. *Journal of Climate*, 29(14), 5175–5188. <https://doi.org/10.1175/JCLI-D-16-0106.1>

Watanabe, M., Dufresne, J.-L., Kosaka, Y., Mauritsen, T., & Tatebe, H. (2021). Enhanced warming constrained by past trends in equatorial Pacific sea surface temperature gradient. *Nature Climate Change*, 11(1), 33–37. <https://doi.org/10.1038/s41558-020-00933-3>

Weijer, W., Cheng, W., Garuba, O. A., Hu, A., & Nadiga, B. T. (2020). CMIP6 models predict significant 21st century decline of the Atlantic meridional overturning circulation. *Geophysical Research Letters*, 47(12), e2019GL086075. <https://doi.org/10.1029/2019GL086075>

Winton, M., Griffies, S. M., Samuels, B. L., Sarmiento, J. L., & Frölicher, T. L. (2013). Connecting changing ocean circulation with changing climate. *Journal of Climate*, 26(7), 2268–2278. <https://doi.org/10.1175/JCLI-D-12-00296.1>

Xie, S.-P., Lu, B., & Xiang, B. (2013). Similar spatial patterns of climate responses to aerosol and greenhouse gas changes. *Nature Geoscience*, 6(10), 828–832. <https://doi.org/10.1038/ngeo1931>

Yeager, S., & Danabasoglu, G. (2014). The origins of late-twentieth-century variations in the large-scale North Atlantic circulation. *Journal of Climate*, 27(9), 3222–3247. <https://doi.org/10.1175/JCLI-D-13-00125.1>

Zhou, C., Zelinka, M. D., & Klein, S. A. (2017). Analyzing the dependence of global cloud feedback on the spatial pattern of sea surface temperature change with a Green's function approach. *Journal of Advances in Modeling Earth Systems*, 9(5), 2174–2189. <https://doi.org/10.1002/2017MS001096>